Available online at www.sciencedirect.com
SCIENCE DIRECT®
ELSEVIER
Earth and Planetary Science Letters xx (2005) xxx–xxx
EPSL
www.elsevier.com/locate/epsl

New evidence for dislocation creep from 3-D geodynamic modeling of the Pacific upper mantle structure

Jeroen van Hunen [a,b,*], Shijie Zhong [b], Nikolai M. Shapiro [b], Michael H. Ritzwoller [b]

[a] *Institute of Geophysics, ETH, Zurich, Switzerland*
[b] *Department of Physics, University of Colorado at Boulder, CO, USA*

Received 15 February 2005; received in revised form 27 June 2005; accepted 5 July 2005

Editor: R.D. van der Hilst

Abstract

Laboratory studies on deformation of olivine in response to applied stress suggest two distinct deformation mechanisms in the earth's upper mantle: diffusion creep through diffusion of atoms along grain boundaries and dislocation creep by slipping along crystallographic glide planes. Each mechanism has very different and important consequences on the dynamical evolution of the mantle and the development of mantle fabric. Due to the lack of in situ observations, it is unclear which deformation mechanism dominates in the upper mantle, although observed seismic anisotropy in the upper mantle suggests the presence of dislocation creep. We examined the thermo-mechanical erosion of the lithosphere by thermal boundary layer instabilities in 3-D dynamical models. This study demonstrates that the seismically derived thermal structure of the Pacific lithosphere and upper mantle imposes an important constraint on the upper mantle deformation mechanism. The predominant deformation mechanism in the upper mantle is dislocation creep, consistent with observed seismic anisotropy. The acceptable activation energy range of 360–540 kJ/mol is consistent with, although at the lower end of, those determined from laboratory studies.

Keywords: plate tectonics; rheology; convection; geodynamical modelling; tomography

1. Introduction

In the last 30 yr, significant progress has been made in determining deformational properties (i.e., rheology) of olivine under laboratory conditions. In particular, with increasing accuracy, experimental studies have determined rheological activation parameters (e.g., activation energy) for wet and dry olivine undergoing diffusion creep and dislocation creep—the two most important deformation mechanisms in the mantle [1–3]. It is important to test the experimental results against in situ mantle processes because the experiments are performed under conditions (e.g., strain rate) that are dramatically different

* Corresponding author. Institute of Geophysics, ETH, Zurich, Switzerland. Tel.: +41 1 633 6623; fax: +41 1 633 1065.
E-mail address: hunen@erdw.ethz.ch (J. van Hunen).

0012-821X/$ - see front matter © 2005 Elsevier B.V. All rights reserved.
doi:10.1016/j.epsl.2005.07.006

from those in the mantle. It is critically important to test which deformation mechanism is predominant in the mantle, given the significance of implications of the mechanism of deformation for the structure and dynamics of the mantle [4]. Post-glacial rebound (PGR) studies reveal that the average mantle viscosity for the top 1200 km of the mantle is about 10^{21} Pa s [5]. However, because of limited resolution, PGR studies cannot distinguish dislocation from diffusion creep mechanisms [1,6]. Other observational constraints on mantle viscosity such as long-wavelength geoid anomalies [7] suffer similar limitations. Only observations of seismic anisotropy in the upper mantle [8,9], if caused by lattice preferred orientation (LPO), suggest the upper mantle being dominated by dislocation creep [1]. Maybe mantle melts and shape-preferred orientation of mantle minerals may also induce anisotropy [1], although these mechanisms are not very likely to cause the globally observed anisotropy.

By contrasting geodynamical models of sub-lithospheric boundary layer instabilities with recent results from seismic tomography of the Pacific upper mantle, this study provides new evidence that the upper mantle is dominated by dislocation creep with an activation energy that is consistent with laboratory values. The thermal structure of the Pacific lithosphere and upper mantle (Fig. 1) is deduced from a 3-D seismological model [10] that has been constructed from a large set of broadband surface wave group [11] and phase [12,13] speed dispersion measurements using a two-step inversion procedure. First, diffraction tomo-

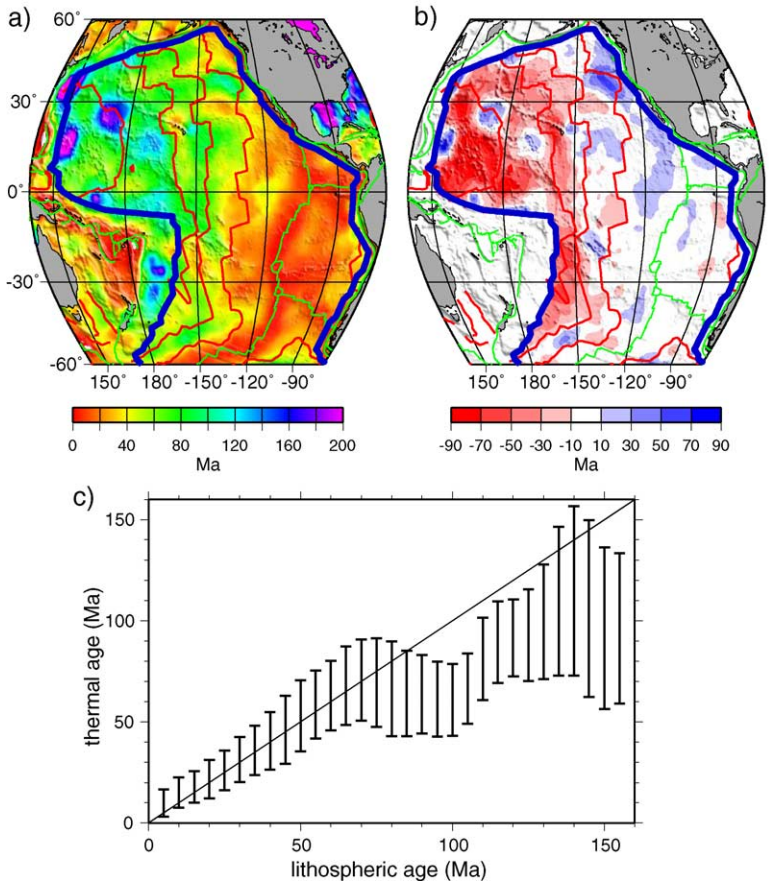

Fig. 1. Seismic results from [10]. a) Apparent thermal age t_a estimated with the seismic inversion (see text for definition of t_a.) b) Difference between lithospheric age t_l and t_a. c) The t_a-distribution for given t_l, collected in 5-Ma age bins. Vertical bars represent standard deviations in age bins from the seismic results.

graphy of [14] was used to construct dispersion maps at periods ranging from 18 to 200 s for group speeds and from 40 to 150 s for phase speeds. This was followed by application of the Monte-Carlo method of Shapiro and Ritzwoller [15] based on a thermal parameterization of upper mantle structure [16] to invert the regionalized dispersion curves for the shear wave speed of the crust and the uppermost mantle on a $2^\circ \times 2^\circ$ grid. A striking feature of the seismic model is that the Pacific lithosphere older than about 70 Ma is significantly hotter than that predicted for a conductively cooling model [17] and that the deviation can be largely explained as a function of lithospheric age t_l. Lithospheric thermal structure is quantified as an "apparent thermal age" t_a [10], which is defined as the lithospheric age at which a purely conductive temperature profile would most closely resemble the observed thermal structure. Comparing apparent thermal age t_a with lithospheric age t_l reveals that (1) t_a approximates t_l for lithosphere younger than about 70 Ma, (2) t_a remains largely unchanged for t_l ranging between 70 and 100 Ma, and (3) t_a increases steadily with t_l for older lithosphere up to 140 Ma (Fig. 1c).

This thermal structure of the Pacific uppermost mantle suggests a period of lithospheric reheating between 70 and 100 Ma and possibly another one after 140 Ma. Physical processes to explain such reheating include both shallow and deep origins. Thermal boundary layer instabilities (TBI) could erode the deeper parts of the lithosphere, as suggested previously on the basis of sea floor topography, gravity and heat flow [18–22]. Although TBI could be triggered by the impingement of mantle plumes [23], the clear age-dependence of the seismic results prompts us to focus on shallower processes—namely, spontaneous TBI [18,24].

Significant progress in the understanding of TBI with realistic mantle rheology has been achieved in the last decade through both laboratory and numerical studies [24–30], which can be summarized as follows. As the lithosphere cools and thickens with time, the bottom part of the lithosphere becomes gravitationally unstable and is eroded by the TBI. The degree of such erosion is determined by the activation energy E^*. Decreasing E^* increases the portion of the lithosphere that is eroded and enhances lithospheric reheating. This is because a smaller E^* leads to a smaller increase in lithospheric viscosity with decreasing temperature and only the portion of lithosphere with viscosity that is less than a factor of 10 larger than the underlying mantle can participate in the TBI and be eroded [24].

In this study, we formulate 3-D mantle convection models with realistic rheology and plate motion to investigate the effects of mantle rheology on the TBI and consequences of the TBI to the lithosphere and upper mantle thermal structure. By comparing with the seismically inferred thermal structure (Fig. 1), we place constraints on mantle rheological properties including the deformation mechanism and activation parameters. We first present the formulation of the convection model and then show how the geodynamic results compare with the seismic model.

2. The convection model

Most numerical studies of convection have been performed in 2-D with diffusion creep deformation (i.e., Newtonian rheology) and no plate motion. To quantify the effects of thermo-mechanical erosion and compare with seismic observations, we formulate a 3-D Cartesian model of mantle convection with the finite element code Citcom [31,32], extended for non-linear (i.e., stress- or strain-rate dependent) rheology. We treat the mantle as an incompressible Boussinesq fluid, for which the non-dimensional governing equations are given as [33]:

$$\nabla \cdot u = 0, \tag{1}$$

$$-\nabla P + \nabla \cdot \left[\eta\left(\nabla \boldsymbol{u} + \nabla^T \boldsymbol{u}\right)\right] + RaTe_z = 0, \tag{2}$$

$$\frac{\partial T}{\partial t} + u \cdot \nabla T = \nabla^2 T, \tag{3}$$

where $\boldsymbol{u}$ describes the material velocity, P the pressure, η the viscosity, T the temperature, and $\boldsymbol{e}_z$ the unit vector in the depth direction. The Rayleigh number Ra is defined as

$$Ra = \frac{\alpha \rho_0 g \Delta T h^3}{\kappa \eta_0} \tag{4}$$

with α, ρ_0, g, ΔT, h, κ, and η_0 being the thermal expansion coefficient, density at unit (non-dimen-

Table 1
Model parameters

Symbol	Description	Value/dimensions
h	Vertical model size	670 km
ΔT	Temperature drop over model	1350 K
ρ_0	Reference density	3300 kg/m^3
κ	Thermal diffusivity	10^{-6} m^2/s
α	Thermal expansion coefficient	3.5×10^{-5}1/K
g	Gravitational acceleration	9.8 m/s^2
R	gas constant	8.3 J/mol

sional) temperature, gravitational acceleration, temperature difference between the top and bottom of the model, height of the model domain, thermal diffusivity, and reference mantle viscosity, respectively. Although dependence of physical parameters such as α on temperature and depth is relevant for large-scale convection [34], the TBI considered here mainly deals with local situations in which variations in pressure and temperature are minor, which allows us to use the Boussinesq approximations, in which all thermodynamic variables are assumed constant, except for ρ in the driving force term. Table 1 describes the dimensional values used in this study. A similar definition is used here for the effective Rayleigh number Ra_{eff}, which uses the effective viscosity in the upper mantle η_{eff} instead of η_0. We used the following non-dimensionalization: length $x=x'h$, time $t=t'h^2/\kappa$, viscosity $\eta=\eta'\eta_0$, and temperature $T=T'\Delta T$.

The model is adapted for the use of both dislocation and diffusion creep deformation mechanisms. For either deformation mechanism, we may use a power-law Arrhenius rheology

$$\dot{\epsilon} = A\sigma^n \exp\left(-E^*/RT_{abs}\right), \quad (5)$$

where $\dot{\epsilon}$, σ, R, T_{abs}, A, and n are the second invariant of strain rate, second invariant of stress, gas constant, absolute temperature, rheology prefactor and exponent, respectively. E^* represents the activation energy and the prefactor A is chosen such that the $\eta_{eff}=\sigma/\dot{\epsilon}=\eta_0$ for the inflow velocity profile at non-dimensional unit temperature. The exponent n is taken to be 1 and 3.5 for diffusion and dislocation creep, respectively. Non-linear rheology implementation is benchmarked against results by Christensen [4].

We solve for the flow and temperature of the oceanic upper mantle down to 670 km depth with an imposed 8.6 cm/yr surface plate motion (Fig. 2). Horizontal dimensions are 14,000 by 2000 km. Flow-through boundary conditions enable inflow of young lithosphere through one side boundary and exiting of old oceanic lithosphere through the opposite side [35]. The temperature at inflow is derived from a half-space cooling model for a 5-Ma old lithosphere. The remaining side boundaries are reflecting. At the top and bottom boundary we impose impermeable no-slip boundary conditions with imposed non-dimensional temperatures of 0 and 1, respectively. This model simulates the cooling of a moving lithosphere and the resulting TBI for prescribed rheological conditions [35]. The model is divided vertically into two rheologically distinct layers: a 410 km thick upper mantle layer where either diffusion or dislocation creep is used and a bottom layer (i.e., transition zone) with diffusion creep. We choose upper mantle viscosity so that the onset of TBI is at approximately 70 Ma [28], consistent with the seismic results [10], and a transition zone viscosity higher by about a factor of up to 50 [7]. The models are time-dependent and we present model results after a statistical steady state is reached.

3. Results of convection models compared with the seismic model

We first present a model in which dislocation creep is the dominant mechanism with $n=3.5$ in the upper

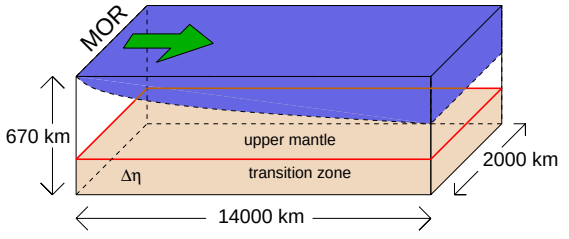

Fig. 2. Schematic model setup of the 3-D numerical calculations. The lithosphere at the surface is prescribed to move with 8.6 cm/yr relative to the non-moving bottom boundary. On the left boundary, Couette-type inflow is defined with a thermal structure corresponding to that of a 5 Ma-old oceanic lithosphere. A constant temperature difference ΔT is maintained between the top and bottom boundary. The upper mantle viscosity is chosen such that TBI initiates at around 70 Ma-old lithosphere. The transition zone (i.e., below 410 km depth) is modeled as a Newtonian fluid (i.e., $n=1$) and has an effective viscosity that is up to 50 times larger than that of the upper mantle.

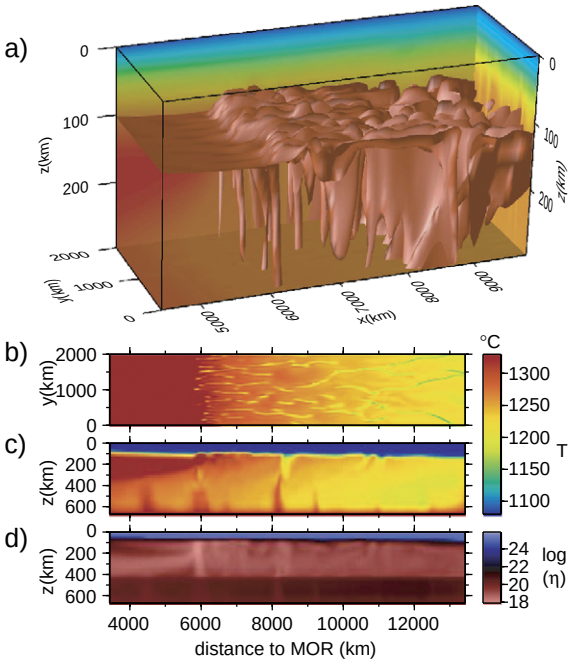

Fig. 3. A representative snapshot of thermal and rheological structures is shown for a model with $E^*=360$ kJ/mol and $n=3.5$. $Ra_{eff}=3\times10^7$ (see text for a definition of Ra_{eff}). a) 3-D view of the temperature field (1250 °C-isotherm) for the top 300 km of the model domain with a 10-fold vertical exaggeration. b) Horizontal temperature cross-section at 150 km depth. c) Vertical temperature cross-section at $y=1000$ km. d) Vertical cross-section of the effective viscosity η at $y=1000$ km. $\eta \approx 1.5\cdot10^{19}$ Pa s in the asthenosphere and about 50 times larger in the transition zone.

mantle to elucidate the effects of the TBI on the thermal and rheological states of the upper mantle and lithosphere (Fig. 3). Rheological parameters for each of the performed model calculations are summarized in Table 2. For this first model, $E^*=360$ kJ/mol and the TBI starts when the lithosphere reaches an age of about 70 Ma or at a distance of about 6000 km from the mid-ocean ridge (MOR). The average effective viscosity in the asthenosphere is 1.5×10^{19} Pa s. The convective structure has a tendency to align with the plate motion, but significant variations exist in directions both perpendicular and parallel to plate motion, particularly at large depths (Fig. 3a–c). At the onset of the TBI, the typical wavelength of structure parallel to plate motion is around 200 km. The wavelength becomes more variable and irregular at larger distances from the MOR, implying significant re-organization of the structure. This structure is sig-

Table 2
Rheological parameters

Model run	A_1 (Pa^{-n} s^{-1})	A_2 (Pa^{-n} s^{-1})	E^* (kJ/mol)	n_1 (−)	n_2 (−)	Ra (−)	η_0 (Pa s)	η_{asth} (Pa s)
1	4.94×10^{-21}	4.22×10^{-9}	360	3.5	1.0	2.40×10^7	1.91×10^{19}	1.45×10^{19}
2	1.33×10^{-14}	4.41×10^{-3}	540	3.5	1.0	3.95×10^7	1.16×10^{19}	1.03×10^{19}
3	1.93×10^{-16}	4.83×10^{-18}	120	1.0	1.0	1.20×10^7	3.83×10^{19}	6.01×10^{19}
4	3.43×10^{-8}	8.57×10^{-10}	360	1.0	1.0	3.90×10^7	1.18×10^{20}	2.13×10^{19}
5	1.93×10^{-16}	3.86×10^{-17}	120	1.0	1.0	1.20×10^7	3.83×10^{19}	5.47×10^{19}

A_1 (n_1) and A_2 (n_2) refer to A (n) in Eq. (5) shallower and deeper than 410 km depth, respectively. η_{asth} represents the asthenospheric viscosity, defined as the minimum value of the horizontally averaged effective viscosity.

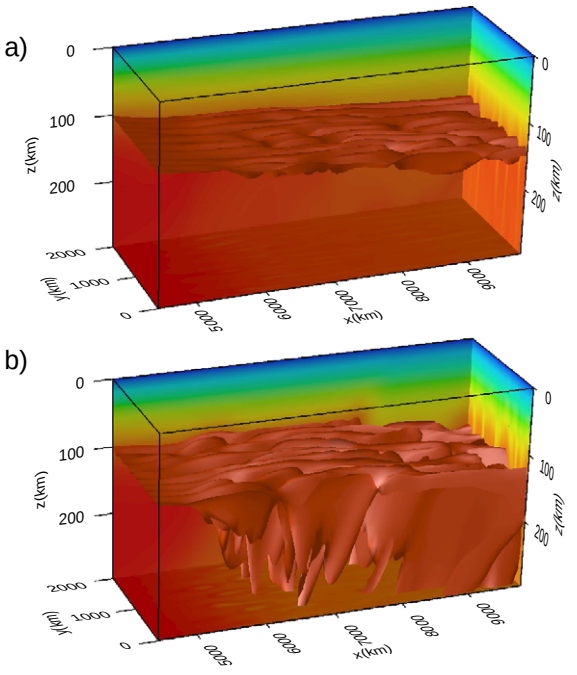

Fig. 4. As in Fig. 3a but showing representative thermal structure for Newtonian models with (a) $E^*=360$ kJ/mol and (b) $E^*=120$ kJ/mol.

nificantly different from the roll structure reported in early laboratory studies of plate-driven instabilities for fluids with relatively uniform properties [36].

The TBI leads to erosion of lithospheric material and an increase in lithospheric temperature (Fig. 3a–c). Consequently, after the onset of TBI, the lithosphere thickens less rapidly or sometimes thins with age. For this model, the 1250 °C-isotherm (as a representative temperature for the bottom of the lithosphere) is lifted up on average by about 15 to 20 km. After this first phase of instability, the lithosphere thickens again, but a difference in thickness with the "undisturbed" lithosphere remains.

In addition, we performed calculations with a linear (i.e. Newtonian, $n=1$) upper mantle rheology. Fig. 4a shows results for an activation energy of 360 kJ/mol; i.e., similar to the case in Fig. 3. TBI in this case shows a more regular roll pattern. The thermal erosion in this case is much smaller: the 1250 °C-isotherm does not show any substantial uplift. Decreasing E^* to 120 kJ/mol (Fig. 4b) enhances thermal erosion. However, the 1250 °C-isotherm is not uplifted as much and the TBI is not as vigorous, compared to the non-Newtonian case (Fig. 3). The difference in thermal erosion between the $n=1$ and $n=3.5$ cases is due to the feedback of the convection into the effective viscosity: at the onset of TBI, the increased deformation rate reduces the effective viscosity due to the non-linear mantle rheology (Fig. 3d), which in turn further enhances the instability. This feedback mechanism creates a convective "avalanche". During this convective episode, the lithosphere is substantially thinned. For the Newtonian rheology, such a feedback mechanism is absent and the thermal erosion is a more continuous process. This also explains the continuous roll structures in the $n=1$ cases (Fig. 4) versus the more irregular convective pattern in the $n=3.5$ case (Fig. 3).

We performed calculations for different values of the activation energy E^* for both diffusion creep ($n=1$) and dislocation creep ($n=3.5$) for the upper mantle (Table 2). All cases display similar dynamics for the TBI. The main difference between cases with different E^* is that reducing E^* increases the thermo-mechanical erosion of the lithosphere. This is consistent with the suggestion that E^* controls temperature anomalies associated with the TBI [24].

To compare these models with each other and with the seismic results we estimate the apparent thermal age t_a at a given lithospheric age t_l or distance to the middle ocean ridge: an averaged temperature is calculated over all lithosphere of given t_l in the top 150 km and over a specified period of time after a statistical steady state is reached. The t_a is the age that gives the same average temperature from a half-space conductive cooling model [17]. For the case with $n=3.5$ and $E^*=360$ kJ/mol, the estimated t_a (Fig. 5) clearly reflects the lithospheric thickness variations: it closely follows lithospheric age t_l until TBI occurs but is reduced during the first phase of TBI before it starts to increase again after about 10 Ma. The t_a remains smaller than t_l by about 25 Ma after an age of 75 Ma. By comparison with other numerical simulations, it is clear that the difference $t_l - t_a$ is a function of E^* with lower E^* resulting in larger discrepancy between lithospheric and apparent thermal ages ($t_l - t_a$).

The different convective behavior between the diffusion and dislocation creep cases is also apparent in the thermal age plot: changes in t_a are more gentle for the $n=1$ case than for the $n=3.5$ case and, for given E^*, $n=3.5$ leads to a larger t_a deviation from t_l. This increasing deviation of t_a from t_l around 70 Ma and

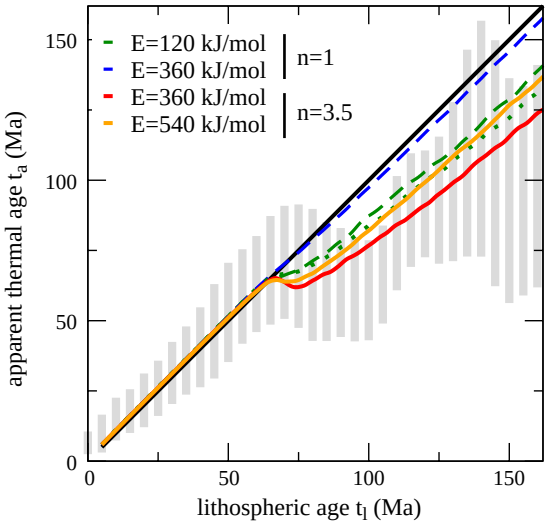

Fig. 5. Apparent thermal age versus lithospheric age from the seismic results (grey bars, also seen in Fig. 1) and numerical model results (lines). Dashed ($n=1$) and solid ($n=3.5$) lines are for a viscosity increase at 410 km depth $\Delta\eta \approx 50$, whereas the dotted line is for $\Delta\eta \approx 5$, $n=1$, and $E^*=120$ kJ/mol for comparison.

the subsequent nearly constant deviation for older lithosphere closely resemble the average seismic thermal structures (Fig. 5) and strongly suggest that the TBI is the mechanism that is responsible for the seismic observations. These results suggest that the seismically derived thermal structure for the Pacific upper mantle can be explained with models with $n=1$ and $E^*=120$ kJ/mol or $n=3.5$ and E^* between 360 and 540 kJ/mol.

4. Discussion and conclusions

We have formulated 3-D numerical models of mantle convection to examine the dynamics of the thermal boundary layer instabilities (TBI) and their influences on lithospheric thermal structure. We demonstrate that the Pacific upper mantle and lithospheric seismic structure [10] can be explained with the TBI with either diffusion creep with $E^* \approx 120$ kJ/mol or dislocation creep with $E^* \approx 360$ to 540 kJ/mol. Estimates of E^* for diffusion creep from experimental studies for olivine aggregates are 375 kJ/mol with 20% uncertainty [3,37], while E^* for dislocation creep is estimated to be 470 and 510 kJ/mol (with 10% uncertainty) for wet and dry conditions, respectively [2,38]. While the experimental estimates of E^* for diffusion creep are much higher than our best fit value of 120 kJ/mol for diffusion creep, for dislocation creep the acceptable range of E^* up to 540 kJ/mol is consistent with laboratory values. This suggests that deformation in the upper mantle beneath the Pacific is accomplished predominantly by dislocation creep and not by diffusion creep.

For the model calculations described above, we used a rheologically layered mantle: diffusion or dislocation creep in the upper mantle down to 410 km depth and a diffusion creep "transition zone" between 410 and 670 km depth with a $\Delta\eta \approx 50$ times higher effective viscosity. Such an effective viscosity profile corresponds well with recent estimates of a transition zone viscosity on the order of 10^{21} Pa s. However, TBI is a local process, which takes place on a scale much smaller than the size of lithospheric plates or the depth extent of the (upper) mantle. It should therefore be relatively insensitive to the circumstances at large lateral distances from the TBI or to deeper mantle conditions. To test the influence of $\Delta\eta$ on the t_a results, we performed a calculation with $n=1$ and $E^*=120$ kJ/mol with a much smaller $\Delta\eta=5$. Fig. 5 shows that values for $t_l - t_a$ are slightly larger in this case. Compared to the case with $\Delta\eta=50$, although the TBI pattern is similar, the reduced $\Delta\eta$ allows cold eroded material to sink and penetrate into the transition zone more easily and results in a slightly higher temperature in the upper mantle, thus affecting t_a. However, because the difference in t_a from calculations with different $\Delta\eta$ is sufficiently small, we conclude that TBI is largely insensitive to the transition zone viscosity. If E^* in Eq. (5) would be replaced by $H^*=E^*+pV^*$, where a non-zero activation volume V^* would give a depth dependence of the total activation enthalpy H^*, the effective viscosity would increase with depth due to dependence on the pressure p. This would reduce the depth extent of the asthenosphere. In the case where this depth extent becomes comparable to or smaller than the lateral size of the TBI (i.e. around 200 km), convection might be hampered due to vertical 'lack of space'. This was also found by Huang et al. [28]. In that case, a higher Rayleigh number Ra might be necessary to enable TBI, but again the effect on the t_a is expected to remain limited.

The rheological parameters in each of the model calculations (Table 2) and effective viscosity can be compared to laboratory predictions, such as those from Karato and Wu [1]. Comparing rheological A-values is only useful, if the other rheological parameters (E^* and n) are the same. Therefore, in our set of calculations, only the A values of calculation 2 (Table 2) can be compared to the dry dislocation creep values from Karato and Wu [1]. For this case, our applied $A=1.33\times10^{-14}$ is about 50 times larger than the laboratory value. The imposed relative plate velocity in our calculation suggests a 'constant strainrate' calculation rather than a 'constant stress' calculation (i.e. if the rheology is changed, mostly the stress changes and less so the strainrate). Eq. (5) then suggests that our effective viscosity

$$\eta_{\mathrm{eff}} = \frac{\sigma}{\dot{\epsilon}} = A^{\frac{-1}{n}}\dot{\epsilon}^{\frac{1-n}{n}}\exp\left[\frac{E^*}{nRT_{\mathrm{abs}}}\right] \quad (6)$$

is about a factor of three smaller than the laboratory dry dislocation creep value. This suggests that the oceanic upper mantle is not completely dry but is affected by some hydrous weakening. A more flexible and qualitative comparison can be made between all model calculations and the minimum effective viscosities in [1, Fig. 2]. Although in our case viscosity increase with depth is controlled by a jump in viscosity at 410 km depth instead of a non-zero activation volume, the asthenospheric viscosity, defined as the minimum effective viscosity (see Table 2, η_{asth}) can still be compared. In most model runs, our asthenospheric viscosity seems to fall in between the dry and wet Karato-and-Wu values.

As a result of the small-scale convection below older lithosphere, the underlying mantle is cooled by about 100 K by the downwellings. Such cooling is observed in earlier studies [24,39,40], although adding internal heating to the model might reduce or even completely compensate for this cooling [40]. This cooling increases the local viscosity, which delays the formation of TBI, but the amount of erosion by TBI is not significantly affected, as discussed above on the basis of two cases with different rates of accumulation of cold downwellings in the upper mantle due to different $\Delta\eta$ values. Even though our model does not provide strong constraints on the amount of mantle cooling due to TBI, it would still be interesting to see if seismic studies indicate such cooling. Although asthenospheric temperatures can be constrained by observing variations in seismic speeds and attenuation [41] or in depths of 400- and 660-km discontinuities [42], the lateral resolution of present-day seismic models in the relevant depth range (200–400 km) remains poor. Future improvement of upper mantle tomography, perhaps by adding more surface-wave overtone data, may resolve this issue.

In addition to explaining the Pacific upper mantle and lithospheric seismic structure, these models of the TBI have other important implications. 1) The dominant deformation mechanism in the upper mantle is dislocation creep, suggesting an LPO-origin for seismic anisotropy and providing further evidence for a relationship between seismic anisotropy and mantle flow and deformation [43]. 2) By reheating the oceanic lithosphere, the TBI process may significantly affect the thermo-mechanical structure of the lithosphere. This may lead to increased heat flux and decreased topographic subsidence (i.e., topographic attening) at relatively old sea floor, compared to the purely conductive cooling model predictions [18]. Although O'Connell and Hager [39] and Davies [44] suggested that by enhancing the cooling of the mantle the TBI may lead to deepened sea floor topography, Huang and Zhong [40] recently demonstrated using mantle convection models with a reasonable internal heating rate that the TBI produces topographic flattening at the surface, supporting the original suggestion by Parsons and McKenzie [18]. 3) The TBI provides an explanation for seismically observed small-scale structures (i.e., smaller than the plate scale) in the upper mantle [45]. We also found that the TBI structure in the upper mantle from non-Newtonian rheology is rather irregular and is significantly different from the roll structure reported in early studies with uniform viscosity structure [36]. Higher-resolution seismic studies that map small-scale upper mantle structures will help further constrain the mantle dynamics and rheology. 4) For certain geodynamic problems non-Newtonian rheology may be approximated with Newtonian rheology but with much reduced activation energy, similar to what Christensen [4] proposed. Our results demonstrate that this simplification is to the first order valid for the thermo-mechanical erosion of lithosphere. Based on modeling exural rigidity observations at

seamounts and oceanic islands with Newtonian rheology for the mantle lithosphere [46], activation energy was inferred to be 120 kJ/mol for the upper mantle, which is consistent with the current study.

Acknowledgments

Two anonymous reviewers helped to improve the manuscript significantly. This study is funded by the David and Lucile Packard Foundation and the US NSF grants EAR 0134939 and EAR 0409217.

References

[1] S.-i. Karato, P. Wu, Rheology of the upper mantle: a synthesis, Science 260 (1993) 771–778 (5).
[2] S.-i. Karato, H. Jung, Effects of pressure on high-temperature dislocation creep in olivine, Philos. Mag. 83 (3) (2003) 401–414.
[3] G. Hirth, D.L. Kohlstedt, The rheology of the upper mantle wedge: a view from experimentalists, in: J. Eiler (Ed.), The Subduction Factory, American Geophysical Union, Washington D.C., 2003.
[4] U.R. Christensen, Convection with pressure and temperature dependent non-Newtonian rheology, Geophys. J. R. Astron. Soc. 77 (1984) 242–284.
[5] J.X. Mitrovica. Haskell [1935] revisited. J. Geophys. Res., 101(B1) (1996) 555–569.
[6] P. Wu, Deformation of an incompressible viscoelastic at earth with powerlaw creep: a finite element approach, Geophys. J. Int. 108 (1992) 35–51.
[7] B.H. Hager, M.A. Richards, Long wavelength variation in earth's geoid: physical models and dynamical implications, Philos. Trans. R. Soc. Lond. 328 (1989) 309–327.
[8] J.-P. Montagner, T. Tanimoto, Global upper mantle tomography of seismic velocities and anisotropies, J. Geophys. Res. 96 (1991) 20337–20351.
[9] G. Ekström, A.M. Dziewonski, The unique anisotropy of the Pacific upper mantle, Nature 394 (1998) 168–172.
[10] M.H. Ritzwoller, N.M. Shapiro, S. Zhong, Cooling history of the Pacific lithosphere, Earth Planet. Sci. Lett. 226 (2004) 69–84.
[11] D.B. Smith, M.H. Ritzwoller, N.M. Shapiro, Stratification of anisotropy in the Pacific upper mantle, J. Geophys. Res. 109 (2004) , doi:10.1029/2004JB003200.
[12] J. Trampert, J.H. Woodhouse, Global phase velocity maps of Love and Rayleigh waves between 40 and 150 s period, Geophys. J. Int. 122 (1995) 675–690.
[13] G. Ekström, J. Tromp, E.W.F. Larson, Measurements and global models of surface waves propagation, J. Geophys. Res. 102 (1997) 8137–8157.
[14] M.H. Ritzwoller, N.M. Shapiro, M.P. Barmin, A.L. Levshin, Global surface wave diffraction tomography, J. Geophys. Res. 107 (2002) 2335, doi:10.1029/2002JB001777.
[15] N.M. Shapiro, M.H. Ritzwoller, Monte-Carlo inversion for a global shear velocity model of the crust and upper mantle, Geophys. J. Int. 151 (2002) 88–105.
[16] N.M. Shapiro, M.H. Ritzwoller, Thermodynamic constraints on seismic inversions, Geophys. J. Int. 157 (2004) 1175–1188.
[17] D.L. Turcotte, G. Schubert, Geodynamics, Applications of Continuum Physics to Geological Problems, Second Edition, Cambridge University Press, 2002.
[18] B. Parsons, D. McKenzie, Mantle convection and thermal structure of the plates, J. Geophys. Res. 83 (1978) 4485–4496.
[19] C.A. Stein, S. Stein, A model for the global variation in oceanic depth and heat flow with lithospheric age, Nature 359 (1992) 123–129.
[20] S. Nagihara, C.R.B. Lister, J.G. Sclater, Reheating of old oceanic lithosphere: deductions from observations, Earth Planet. Sci. Lett. 139 (1996) 91–104.
[21] W.F. Haxby, J.K. Weissel, Evidence for small-scale mantle convection from SEASAT altimetry data, J. Geophys. Res. 91 (1986) 3507–3520.
[22] W.R. Buck, E.M. Parmentier, Convection beneath young oceanic lithosphere: implications for thermal structure and gravity, J. Geophys. Res. 91 (1986) 1961–1974.
[23] W.B. Moore, G. Schubert, P. Tackley, Three-dimensional simulations of plume–lithosphere interaction at the Hawaiian swell, Science 279 (1998) 1008–1011.
[24] A. Davaille, C. Jaupart, Onset of thermal convection in fluids with temperature-dependent viscosity: application to the oceanic mantle, J. Geophys. Res. 99 (1994) 19853–19866.
[25] C.P. Conrad, P. Molnar, Convective instability of a boundary layer with temperature- and strain-rate-dependent viscosity in terms of available buoyancy, Geophys. J. Int. 139 (1999) 51–68.
[26] G. Marquart, On the geometry of mantle flow beneath drifting lithospheric plates, Geophys. J. Int. 144 (2001) 356–372.
[27] C. Dumoulin, M.-P. Doin, L. Fleitout, Numerical simulation of the cooling of an oceanic lithosphere above a convective mantle, Phys. Earth Planet. Inter. 125 (2001) 45–64.
[28] J. Huang, S. Zhong, J. van Hunen, Controls on sub-lithospheric small-scale convection, J. Geophys. Res. 108 (B8) (2003) 2405, doi:10.1029/2003JB002456.
[29] J. Korenaga, T.H. Jordan, Physics of multi-scale convection in the earth's mantle. Onset of sublithospheric convection, J. Geophys. Res. 108 (B7) (2003) 2333, doi:10.1029/2002JB001760.
[30] S.E. Zaranek, E.M. Parmentier, The onset of convection in fluids with strongly temperature-dependent viscosity cooled from above with implications for planetary lithospheres, Earth Planet. Sci. Lett. 224 (2004) 371–386.
[31] L. Moresi, M. Gurnis, Constraints on the lateral strength of slabs from three-dimensional dynamic flow models, Earth Planet. Sci. Lett. 138 (1996) 15–28.
[32] S. Zhong, M.T. Zuber, L. Moresi, M. Gurnis, Role of temperature-dependent viscosity and surface plates in spherical

shell models of mantle convection, J. Geophys. Res. 105 (B8) (2000) 11063–11082.
[33] D.P. McKenzie, J.M. Roberts, N.O. Weiss, Convection in the mantle: towards a numerical simulation, J. Fluid Mech. 62 (1974) 465–538.
[34] H. Schmeling, G. Marquart, T. Ruedas, Pressure- and temperature-dependent thermal expansivity and the effect on mantle convection and surface observables, Geophys. J. Int. 154 (2003) 224–229.
[35] J. van Hunen, J. Huang, S. Zhong, The effect of shearing on the onset and vigor of small-scale convection in a Newtonian rheology, Geophys. Res. Lett. 30 (19) (2003) 1991, doi:10.1029/2003GL018101.
[36] F.M. Richter, B. Parsons, On the interaction of two scales of convection in the mantle, J. Geophys. Res. 80 (1975) 2529–2541.
[37] S. Mei, D.L. Kohlstedt, Influence of water on plastic deformation of olivine aggregates: 1. Diffusion creep regime, J. Geophys. Res. 105 (2000) 21457–21469.
[38] S. Mei, D.L. Kohlstedt, Influence of water on plastic deformation of olivine aggregates: 2. Dislocation creep regime, J. Geophys. Res. 105 (2000) 21471–21481.
[39] R.J. O'Connell, B.H. Hager, On the thermal state of the earth, in: A. Dziewonski, E. Boschi (Eds.), Physics of the Earth's Interior, 1980, pp. 270–317.
[40] J. Huang, S. Zhong, Sublithospheric small-scale convection and its implications for the residual topography at old ocean basins and the plate model, J. Geophys. Res. 110 (2005) B05404, doi:10.1029/2004JB003153.
[41] Y. Gung, B. Romanowicz, Superplumes from the core–mantle boundaries to the lithosphere, Science 296 (2003) 513–516.
[42] P.M. Shearer, Upper mantle seismic discontinuities, in: S. Karato, A.M. Forte, R.C. Liebermann, G. Masters, L. Stixrude (Eds.), Earth's Deep Interior: Mineral Physics and Tomography from the Atomic to the Global Scale, Am. Geophys. Un., 2000, pp. 115–131.
[43] P.G. Silver, W.E. Holt, The mantle flow field beneath western North America, Science 295 (2002) 1054–1057.
[44] G.F. Davies, Ocean bathymetry and mantle convection 2. Small-scale flow, J. Geophys. Res. 93 (1988) 10481–10488.
[45] R. Katzman, L. Zhao, T.H. Jordan, High-resolution, two-dimensional vertical tomography of the central Pacific mantle using ScS reverberations and frequency-dependent travel times, J. Geophys. Res. 103 (1998) 17933–17971.
[46] A.B. Watts, S. Zhong, Observations of exure and the rheology of oceanic lithosphere, Geophys. J. Int. 142 (2000) 12177–12190.